STIFF LATTICES WITH ZERO THERMAL EXPANSION AND ENHANCED STIFFNESS VIA RIB CROSS SECTION OPTIMIZATION

Jeremy Lehman[1*] and Roderic Lakes[2]

1 Engineering Mechanics Program;
2 Department of Engineering Physics, Materials Science Department and Rheology Research Center,
University of Wisconsin-Madison
1500 Engineering Drive, Madison, WI 53706-1687
* address correspondence to JL: e-mail- jjlehman@wisc.edu

Preprint 4 June 2012 for
J.J. Lehman and R.S. Lakes, "Stiff lattices with zero thermal expansion and enhanced stiffness via rib cross section optimization" *Int. J. Mech. Mater. Des.* 9, (3), 213-225 (2013).

ABSTRACT

Honeycombs with thermal expansion coefficients equal to zero are described analytically. The two dimensional lattice microstructure designs described are made of positive expansion materials. This work builds upon previous results, and provides further analysis into creating an optimal rib cross section. The design of ribs with Tee shaped and I shaped cross sections is developed. The behavior of these lattices is compared with that of triangular and hexagonal honeycombs as well as prior rectangular lattice results in a modulus-density map. Lattice relative stiffness is improved by as much as a factor of 2.4 when compared with a curved triangular lattice with ribs of rectangular section. Thermal shear stress at the material interface is found to be small. These lattices do not undergo thermal buckling, in contrast to designs based on sub-lattices.

INTRODUCTION

A material's coefficient of thermal expansion (CTE) is an important factor when selecting materials for applications with large temperature variations (Sokolnikoff, 1983). For these applications dimensional stability can be achieved by designing a material of near zero thermal expansion. According to Cribb (1968), the CTE of two phase composites are limited to a weighted average of the coefficients of thermal expansion of the two constituents, based on the volume fraction and bulk moduli of the two phases. This model prevents the composite CTE from being larger or smaller than either component phase and thus zero thermal expansion is not possible without a negative CTE material. These CTE bounds in addition to bounds (Hashin, 1983; Milton, 2002; Paul, 1960) for elastic moduli of two phase composites are based on the assumption that the phases are perfectly bonded, have positive definite strain energy and that the composite is not porous. The bounds can be exceeded by relaxing these assumptions. Zero or large positive or large negative thermal expansions are possible in composite materials with void spaces, and by careful design of their micro structure (Lakes, 1996, 2007). The present manuscript describes the design and analysis of two dimensional lattices made of curved bi-material rib elements that are capable of achieving zero thermal expansion. The lattices are optimized for stiffness by varying the cross sectional shape of their rib elements. Lattice structures are compared to prior lattices including those with ribs of different materials.

Previous analysis has been performed to provide a method to calculate the overall thermal expansion coefficient (CTE) and mechanical stiffness of the entire 2D lattice (Lehman and Lakes, 2012). These results are applicable to triangular honeycomb lattices constructed of curved, bi-material rib elements. The structure of each rib element is made of two different metals each with different positive thermal expansion coefficients. This difference of thermal expansion coefficients results in bending of the element, which causes a reduction of the distance between the ends of the rib element. By carefully specifying geometric parameters including a slight initial curvature, the material's thermal elongation can be counteracted, resulting in a honeycomb or lattice structure of zero thermal expansion. The following Equations (1-2) were obtained previously and are only applicable to ribs with a rectangular cross section and provide the overall thermal expansion coefficient (α) and mechanical stiffness E_H (Lehman and Lakes, 2012).

$$\alpha = (\alpha_1 - \alpha_2)\frac{L_{arc}}{t}\left(\frac{\theta}{12}\right)\frac{6(1+m)^2}{3(1+m)^2 + (1+mn)\left(m^2 + \frac{1}{mn}\right)} + \frac{\alpha_1 + \alpha_2}{2} + (\alpha_2 - \alpha_1)\left[\frac{4m^2 + 3m + \frac{1}{nm}}{nm^3 + 4m^2 + 6m + \frac{1}{nm} + 4} - \frac{1}{2}\right] \quad \textbf{(1)}$$

$$E_H = \frac{2}{\sqrt{3}}\left(\frac{t}{L_{arc}}\right)\frac{E_1 m + E_2}{m+1}\left[\frac{2\theta^3}{24\left(\frac{L_{arc}}{t}\right)^2\left(\frac{\theta}{2}\cos(\theta) + \theta - \frac{3}{2}\sin(\theta)\right) + 3\theta^2\sin(\theta) - \theta^3}\right] \quad \textbf{(2)}$$

in which θ represents the included angle, t is the total thickness of the rib element, L_{arc} is the length of the rib element, E_1 and E_2 are the Young's Moduli of materials one and two, α_1 and α_2 are the CTEs of materials one and two, m is the thickness ratio of material one to material two, and n is the Young's Modulus ratio of material one to material two. To achieve zero thermal

expansion, material one is required to have a smaller CTE and to be positioned on the inner portion of the curved element.

In order to maximize mechanical stiffness a triangular honeycomb lattice was chosen and analyzed, as is shown in **Figure 1** (Lehman and Lakes, 2012).

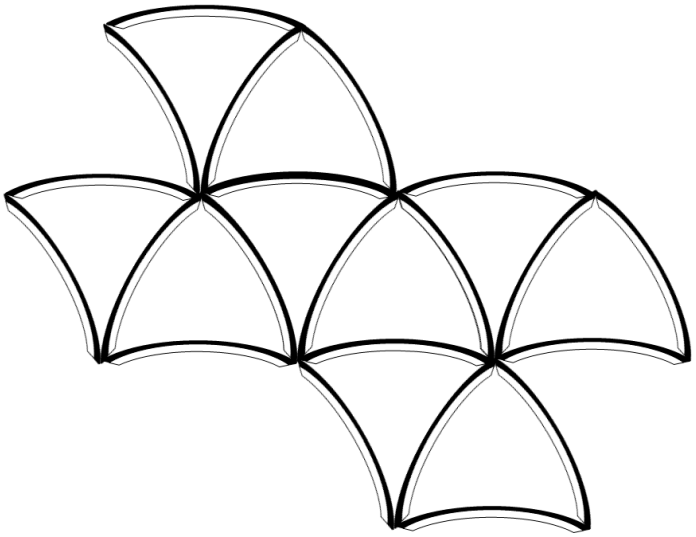

Figure 1 shows the chosen lattice design consisting of curved, bi-material rib elements. Material one is designated in white, while material two is shown in black. This lattice structure is the same as the one previous analysis (Lehman and Lakes, 2012) except the rib cross section shape is optimized in the present analysis.

This lattice allows an overall expansion coefficient of zero, at the cost of a moderate stiffness reduction. The stiffness reduction is attributed to bending deformation as a result of the rib element's slight curvature. An optimally stiff lattice structure is stretch dominated with no bending of ribs, such as a straight-rib, triangular lattice structure.

The reduction in stiffness due to bending can be mitigated by specifying a modified cross section of each rib element. Both Tee and I shaped sections are studied. Modified equations for overall thermal expansion and stiffness moduli are provided, as well as a study of interfacial shear stress. Results are compared to previous results (Lehman and Lakes, 2012) and to prior triangular and hexagonal lattices.

CROSS SECTION DESIGN

It is possible to increase the mechanical stiffness of the lattice structure by altering the shape of an individual rib element's cross section. For previous analyses (Lehman and Lakes, 2012) the cross section has been assumed to be rectangular, with the thickness specified as t and the width fixed as unit length. The parameters that are allowed to be varied are a_1 and a_2, corresponding to the respective material thicknesses. The ratio of variables a_1 to a_2 is defined by m. **Figure 2** illustrates the cross section and its defining parameters specified for a simple rectangular cross section.

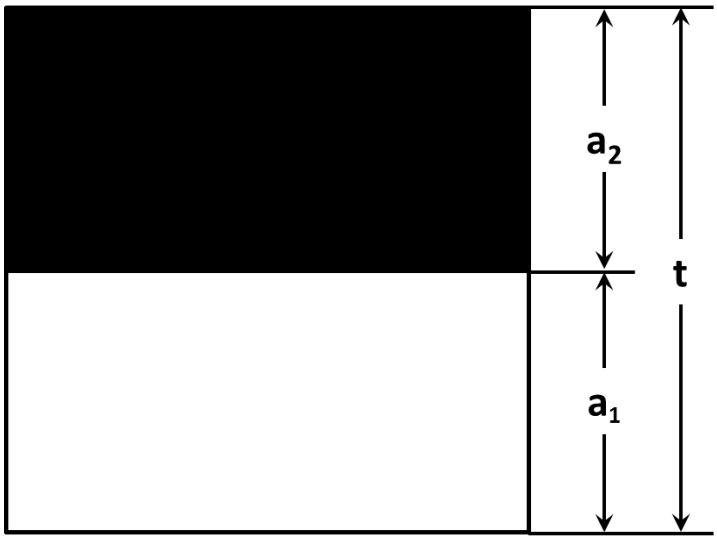

Figure 2 shows the rectangular cross section and its defining parameters shown where $m = a_1/a_2$ is equal to one.

It is desirable to modify the cross section to a shape that better resists bending, which is a significant cause for stiffness reduction. This analysis allows the cross section to be modified into both Tee and I-sections.

To create a Tee-section, the assumption that the two materials are of equal width is relaxed. The analysis requires the addition of two dimensions (b_1 and b_2) and one dimensionless parameter (j). b_1 and b_2 represent the respective widths of materials one and two and *j* is the ratio of the width of material one to material two ($j = b_1/b_2$). The dimensionless parameter *j* is able to be any positive number, but is restricted by the effect of the size of the material interface. The larger the deviation of *j* from one the smaller the material interface on the interfacial stress that results from temperature change. If *j* is equal to one the previous rectangular section is obtained. **Figure 3** shows a Tee cross section with all of its characteristic parameters. The following analysis varies these parameters in order to obtain an optimal design, while restricting the cross sectional area to remain constant.

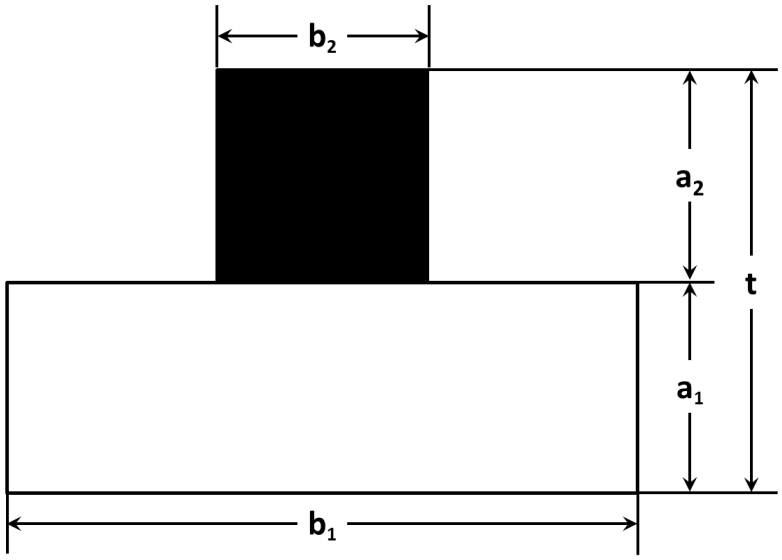

Figure 3 shows a Tee-section with its defining parameters, where *m* equals one and $j = b_1/b_2$ equals three.

An I section can be created by specifying two additional dimensions and two additional dimensionless ratios. I-sections used in this analysis are constrained to have flanges of equal width (b_1), but allow for varying flange thicknesses. The flange thicknesses for material one and material two are specified by c_1 and c_2 respectively. The newly defined dimensionless ratios are k_1 and k_2 where k_1 is the ratio of c_1 over a_1 and k_2 is the ratio of c_2 over a_2. The values of these new ratios can vary between zero and one. If the value of k_1 is equal to one and k_2 equals zero than the section becomes a Tee-section, specified as it is in **Figure 3**. Furthermore if the value of j is equal to one a rectangular section is specified. This allows the I-section solution to be compared to the previous results for these special cases. **Figure 4** illustrates the dimensioning scheme used for the I-section analysis.

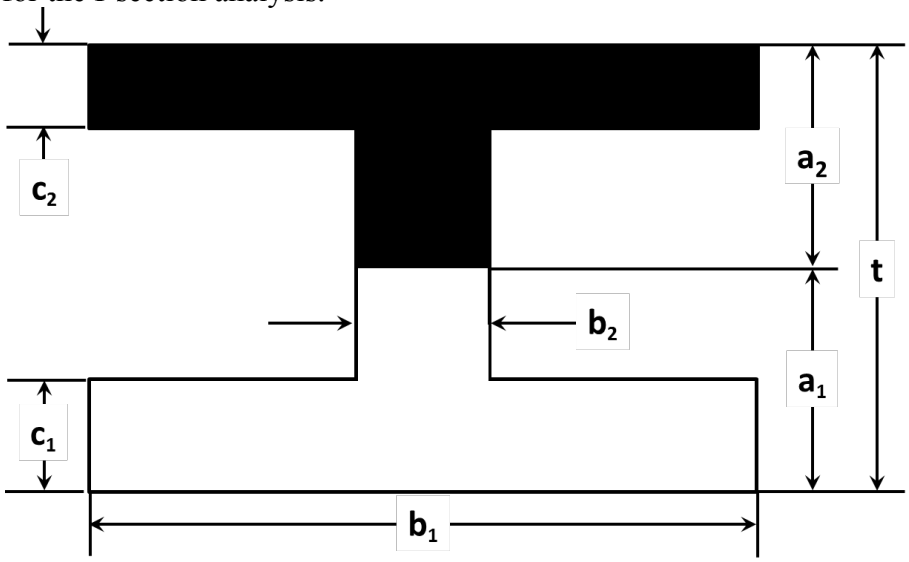

Figure 4 shows the relevant dimensions for a typical I shaped cross section.

RESULTS

The analysis of Tee-section and I-section rib elements follows that of rectangular cross sections, while allowing for additional geometry parameters. Throughout the analysis the cross sectional area remains constant as the parameters j, k_1, and k_2 are varied. That is to say the area already existing is merely redistributed to create either a Tee or I shape. This allows for a meaningful comparison of lattices for differing parameters since the overall cross section does not change in size.

The analysis makes use of several assumptions. The standard elementary beam bending assumptions of a slender bar subjected to small deformations are applied. The material interface is assumed to have no slip. The lattice structure is assumed to be connected by pin joints, and the rib elements do not interfere with one another. Small angle approximations are made resulting in a 5% error in thermal expansion for included angles equal to 0.62 radians. Additionally it is assumed that material properties do not vary with time or temperature. The following analysis first modifies the previous equation for thermal expansion, and then that of overall stiffness. An equation for thermal shear stress at the material interface is derived for a subset of cross sections.

Thermal Expansion Coefficient α of a Tee-Section

The thermal expansion coefficient can be determined by simply replacing the values for material one and two's moment of inertia and cross sectional area in Timoshenko's (1925) equations. These modifications result in new formulas for the change in curvature as well as overall thermal expansion. For instance, the area of material one is changed from a_1 for a rectangular cross section to a_1 times b_1. Equation 3 provides the area moments of inertia used for materials one and two.

$$I_1 = \frac{1}{12} b_1 a_1^3 , \; I_2 = \frac{1}{12} b_2 a_2^3 \tag{3}$$

From these formulas and Timoshenko's (1925) relationships, the change in curvature can be determined to be as shown in Equation 4 for a given change in temperature (ΔT).

$$\frac{1}{\Delta\rho} = \frac{6\left(\alpha_2 - \alpha_1\right)(m+1)^2 \Delta T}{t\left(3(m+1)^2 + (j\,m\,n+1)\left(m^2 + \frac{1}{j\,m\,n}\right)\right)} \tag{4}$$

Using the relationship for the change in curvature it is possible to determine the thermal expansion due to bending, the derivation of which follows closely that of previous analysis (Lehman and Lakes, 2012). Equation 5 relates the expansion due to bending for a T shaped cross section, using small angle approximations.

$$\alpha_{Bend} = \left(\alpha_1 - \alpha_2\right) \frac{L_{arc}}{t} \left(\frac{\theta}{12}\right) \frac{6(m+1)^2}{3(m+1)^2 + (mnj+1)\left(m^2 + \frac{1}{mnj}\right)} \tag{5}$$

Equation 5 leads to a negative bending contribution if the thermal expansion coefficient of material one is less than that of material two, where material one is located on the inside of the curved rib element. This effect is counteracted by the lengthwise growth of the rib element. This lengthwise or axial thermal expansion can be described by Equation 6. The derivation of Equation 6 follows the axial expansion derivation used in earlier analysis (Lehman and Lakes, 2012), and uses the longitudinal strain equations given by Timoshenko (1925).

$$\alpha_{Axial} = \frac{\alpha_1 + \alpha_2}{2} + \left(\alpha_2 - \alpha_1\right)\left[\frac{4m^2 + 3m + \frac{1}{mnj}}{m^3 nj + 4m^2 + 6m + \frac{1}{mnj} + 4} - \frac{1}{2}\right] \quad \textbf{(6)}$$

Equation 6 produces a positive longitudinal expansion given that both materials have a positive coefficient of thermal expansion. This relationship assumes that the included angle is small which is valid for the range of curvatures studied.

To obtain an overall thermal expansion coefficient for an individual rib element and thus the total curved triangular lattice the bending and axial contributions can simply be added to one another. Equation 7 provides a formula to determine the overall thermal expansion coefficient (α).

$$\alpha = \left(\alpha_1 - \alpha_2\right)\frac{L_{arc}}{t}\left(\frac{\theta}{12}\right)\frac{6(m+1)^2}{3(m+1)^2 + (mnj+1)\left(m^2 + \frac{1}{mnj}\right)} + \frac{\alpha_1 + \alpha_2}{2} + \left(\alpha_2 - \alpha_1\right)\left[\frac{4m^2 + 3m + \frac{1}{mnj}}{m^3 nj + 4m^2 + 6m + \frac{1}{mnj} + 4} - \frac{1}{2}\right] \quad \textbf{(7)}$$

By carefully selecting material and geometric parameters, the above equation can be tuned to obtain a zero thermal expansion. It should be noted that by specifying a rectangular cross section ($j = 1$) Equation 7 reduces to the previous solution given by Equation 1.

Equation 7 provides the capability to improve the overall lattice stiffness by requiring less initial curvature to obtain zero expansion as well as increasing the bending stiffness of the individual rib elements. **Figure 5** illustrates the effect of j on the included angle required to achieve a CTE of zero. This plot was generated using typical material values of Invar for material one, and steel for material two. The rib aspect ratio (AR) or the length to thickness ratio is a constant value of 10. The invar thickness percentage (a_1/t) is varied numerically while the overall expansion is constrained to be zero.

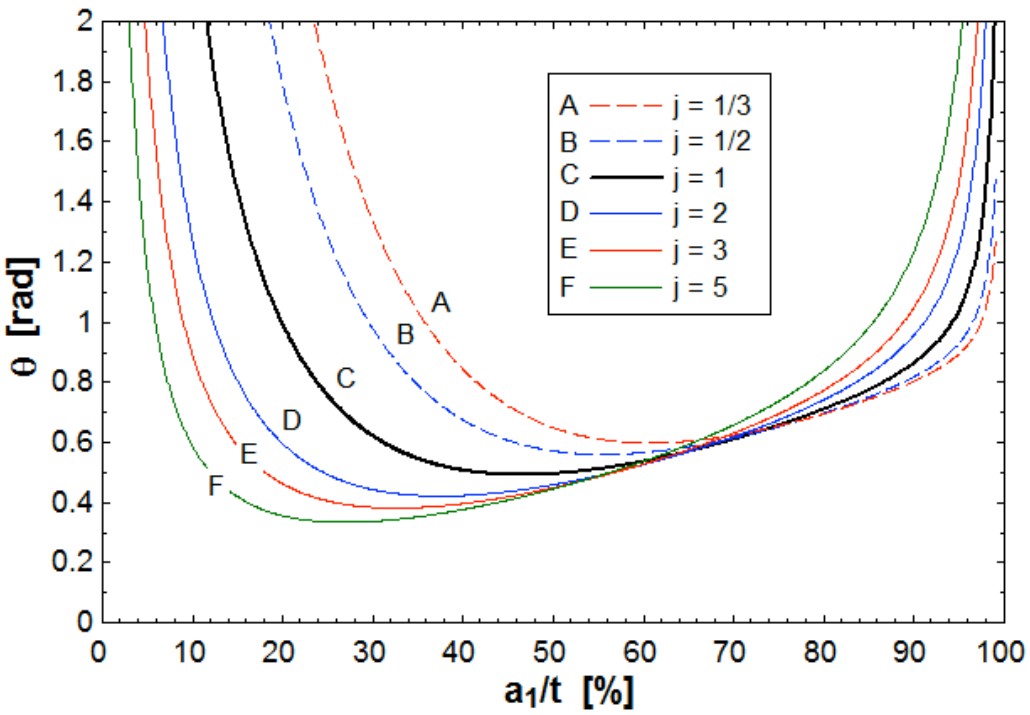

Figure 5 shows the impact of varying section dimension ratio *j* upon the required angle θ for an aspect ratio of 10 to achieve a zero thermal expansion in latttices with Tee section ribs.

From **Figure 5** it can be seen that increasing the width ratio *j* allows for a smaller initial curvature. Conversely, reducing *j* leads to a larger minimum initial curvature. In addition the optimum thickness percentage of material one changes with changing *j*. This implies that a higher value for *j* will result in an overall more rigid lattice. This formula is limited in applicability by the assumption of slenderness, no-slip interface at the material boundary as well as the small angle approximation.

Lattice Elastic Modulus of a Tee-Section

The total elastic modulus (E_H) is found by following a process similar to that of the rectangular cross section, with modifications to allow for the additional obtainable geometry. This analysis restricts the total cross sectional area to remain constant. This ensures an equitable comparison between various rib geometries. A new deformation (δ) in terms of applied load *P* is found by applying standard curved beam equations found in *Roark's Formulas for Stress & Strain* (Young, 1989). Equation 8 provides the deformation in the chord direction for a curved bi-material rib with a T-shaped cross section. The formula neglects shear effects which are small for slender beams.

$$\delta_{sum} = P\left(\frac{L_{arc}}{t}\right)^3 \frac{12(mj+1)^2(m+1)^2}{(E_1 mj + E_2)\left(m^3 j + \frac{3mj(m+1)^2}{mj+1} + 1\right)}\left[\frac{\cos^2\left(\frac{\theta}{2}\right)+\frac{1}{2}}{\theta^2} - \frac{3\sin\left(\frac{\theta}{2}\right)\cos\left(\frac{\theta}{2}\right)}{\theta^3}\right] - P\left(\frac{L_{arc}}{t}\right)\frac{mj+1}{E_1 mj + E_2}\left[\frac{1}{2} - \frac{3\sin\left(\frac{\theta}{2}\right)\cos\left(\frac{\theta}{2}\right)}{\theta}\right] \quad \textbf{(8)}$$

The previous equation for deformation valid for a rectangular cross section is obtained when *j* is equal to 1. Using Equation 8 and following the methods outlined by Hunt (1993), the total mechanical stiffness for a curved triangular lattice can be found. Equation 9 provides the

relationship for the overall lattice Young's modulus. The derivation treats the ribs as pin connected, allowing rotation about the lattice nodes.

$$E_H = \frac{2}{\sqrt{3}}\left(\frac{t}{L_{arc}}\right)\frac{(E_1 mj + E_2)\left(m^3 j + \frac{3mj(m+1)}{mj+1}^2 + 1\right)}{mj+1}\left[\frac{2\theta^3}{24\left(\frac{L_{arc}}{t}\right)^2 (mj+1)(m+1)^2\left(\frac{\theta}{2}\cos(\theta) + \theta - \frac{3}{2}\sin(\theta)\right) + \left(m^3 j + \frac{3mj(m+1)}{mj+1}^2 + 1\right)\left(3\theta^2 \sin(\theta) - \theta^3\right)}\right] \quad \textbf{(9)}$$

Figure 6 illustrates the effect of *j* on overall lattice stiffness. The plot was generated by specifying an aspect ratio of ten, zero thermal expansion, typical values of modulus and CTE for Invar and steel, and then varying the thickness fraction of material one (Invar). Each curve represents a different *j* value.

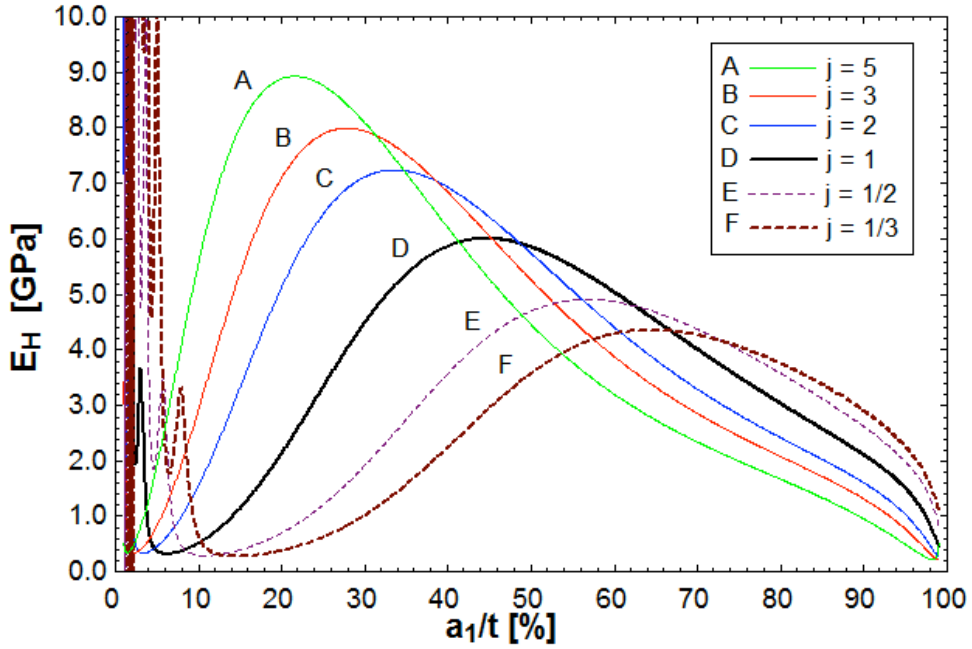

Figure 6 shows Tee section lattice Young's modulus versus Invar thickness fraction for curves A-F representing different values of rib section dimension ratio j. The lattice has zero thermal expansion.

Figure 6 indicates that larger *j* values give rise to larger optimal Young's moduli. These optimum values occur at smaller and smaller Invar height fractions. The *j* value is limited by practical concerns from assuming no slip conditions at the material interface and manufacturing considerations. A comparison can be made with other honeycomb lattice structures. This is done by plotting relative stiffness (E_H / E_S) versus relative density (ρ^* / ρ_S) in which the subscript s indicates the solid rib material. Relative density for a curved triangular lattice is given by Equation 10.

$$\frac{\rho^*}{\rho_S} = \frac{\sqrt{3}}{2}\frac{\theta^2}{\sin^2\left(\frac{\theta}{2}\right)}\frac{t}{L_{arc}} \quad \textbf{(10)}$$

Figure 7 compares the relative stiffness ratios versus relative densities for several lattices. The dashed lines represent either an equilateral triangular lattice or a regular hexagon lattice, the equations for which come from Gibson and Ashby (1997).

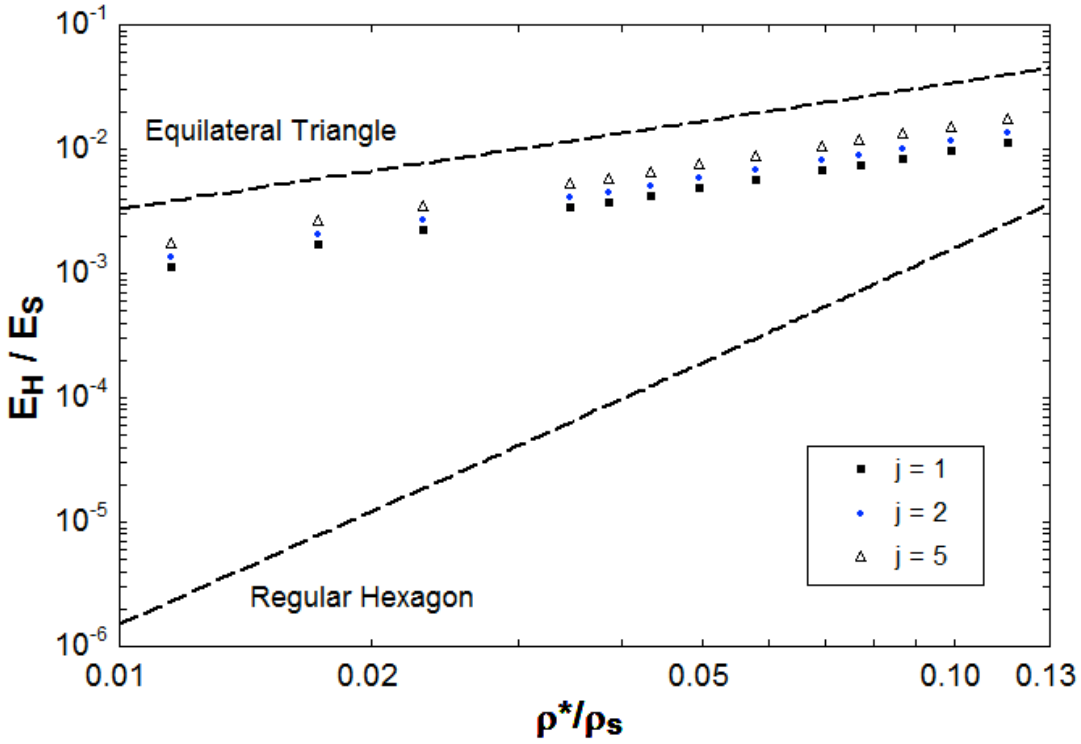

Figure 7 compares relative stiffness versus relative density for different lattice geometries including triangular lattices with Tee-cross sections of optimal ratio a_1/t.

The equilateral triangle lattice represents a purely axially dominant structure while a hexagonal lattice is bending dominant. The data points represent curved, bi-material, triangular lattices. As the value of *j* increases the lattice shifts toward the fully axially dominated triangular lattice. The value of m is optimized to obtain zero thermal expansion. Design of the rib cross section gives rise to an improvement in relative stiffness of as much as a factor of 1.6 for a *j* value of 5.

Thermal Expansion Coefficient α of an I-Section

The same analysis is performed for an I-section. Timoshenko's (1925) equations are applied to determine the curvature. Modifications to these are made to accommodate different values for area, area moment of inertia, and newly located neutral axes of the two materials. From the expected change in curvature both an axial and bending contribution can be obtained. Because of the more complex nature of the geometry a large number of terms exist in the derived equations. For this reason only the final total thermal expansion result is presented. Additionally a sequence of four X coefficients has been defined to reduce the size of any single expression. Each X coefficient is entirely dependent upon specified cross sectional geometry and is non-dimensional. The expressions for these coefficients as well as that for the overall thermal expansion are given by Equations 11-15.

$$X_1 = \frac{X_3}{k_2(j-1)+1}\left[mn\left(k_1(j-1)+1\right)+ k_2(j-1)+1\right] \qquad \textbf{(11)}$$

$$X_2 = \frac{1}{m+1}\left[\frac{m\left[\frac{1}{2}(1-k_1)^2+jk_1\left(1-\frac{k_1}{2}\right)\right]}{k_1(j-1)+1}+\frac{\frac{1}{2}(1-k_2)^2+jk_2\left(1-\frac{k_2}{2}\right)}{k_2(j-1)+1}\right] \quad \textbf{(12)}$$

$$X_3 = \frac{m^2}{(m+1)^2}\left[\frac{j k_1^3+(1-k_1)^3}{12\left(k_1(j-1)+1\right)}+\frac{j k_1(1-k_1)}{4\left(k_1(j-1)+1\right)^2}\right]+\frac{1}{mn\,(m+1)^2\left[k_1(j-1)+1\right]}\left[\frac{j k_2^3+(1-k_2)^3}{12}+\frac{j k_2(1-k_2)}{4\left(k_2(j-1)+1\right)^2}\right] \quad \textbf{(13)}$$

$$X_4 = \frac{m\left[\frac{1}{2}(1-k_1)^2+j k_1\left(1-\frac{k_1}{2}\right)\right]}{(m+1)\left[k_1(j-1)+1\right]} \quad \textbf{(14)}$$

$$\alpha = (\alpha_1-\alpha_2)\frac{L_{arc}}{t}\left(\frac{\theta}{12}\right)\frac{X_2}{X_2^2+X_1}+\frac{\alpha_1+\alpha_2}{2}+(\alpha_2-\alpha_1)\left[\frac{X_3+X_2X_4}{X_2^2+X_1}-\frac{1}{2}\right] \quad \textbf{(15)}$$

Equation 15 follows previous results containing both a bending component and an axial component which serve to counteract one another. By specifying k_1 equal to one and k_2 equal to zero, the Tee-section result is obtained. Additionally by constraining j to be equal to one the previous rectangular result is obtained.

Lattice Elastic Modulus of an I –Section

The stiffness modulus derivation for a curved rib lattice with I-shaped cross sections follows that used for the Tee-section. The notable changes include modifying the relationships used to define the areas, area moment of inertia and neutral axis of the new geometry. The complicated geometric properties are simplified by defining a sequence of dimensionless terms, for this analysis X_5 through X_9 are used. Equations 16-21 define these dimensionless parameters and the total stiffness modulus.

$$X_5 = \sqrt{m\left(k_1(j-1)+1\right)}\left[\frac{m^2\left(k_1^2(j-1)+1\right)-k_2(j-1)\left(k_2-2(m+1)\right)+2m+1}{2\left[m\left(k_1(j-1)+1\right)+k_2(j-1)+1\right]}+\frac{m\left[(j-1)\left(k_1-\frac{k_1^2}{2}\right)+\frac{1}{2}\right]}{k_1(j-1)+1}\right] \quad \textbf{(16)}$$

$$X_6 = \sqrt{k_2(j-1)+1}\left[m+\frac{(j-1)\left(k_2-\frac{k_2^2}{2}\right)+\frac{1}{2}}{k_2(j-1)+1}-\frac{m^2\left(k_1^2(j-1)+1\right)-k_2(j-1)\left(k_2-2(m+1)\right)+2m+1}{2\left[m\left(k_1(j-1)+1\right)+k_2(j-1)+1\right]}\right] \quad \textbf{(17)}$$

$$X_7 = m^3\left(\frac{j k_1^3+(1-k_1)^3}{12}+\frac{j k_1(1-k_1)}{4\left(k_1(j-1)+1\right)}\right)+\frac{j k_2^3+(1-k_2)^3}{12}+\frac{j k_2(1-k_2)}{4\left[k_2(j-1)+1\right]} \quad \textbf{(18)}$$

$$X_8 = (m+1)^2\left[(j-1)(m k_1+k_2)+m+1\right] \quad \textbf{(19)}$$

$$X9 = \frac{X8}{(m+1)^2\left[(j\text{-}1)(mn\,k1 + k2) + mn + 1\right]} \quad \textbf{(20)}$$

$$E_H = \frac{4\,E2}{\sqrt{3}\,X9}\left(\frac{t}{Larc}\right)^3\left[\frac{\theta^3}{\frac{X8}{X5^2 + X6^2 + X7}\left(\theta\left(\cos(\theta) + 2\right) - 3\sin(\theta)\right) + \left(\frac{t\,\theta}{Larc}\right)^2\left(3\sin(\theta) - \theta\right)}\right] \quad \textbf{(21)}$$

Equation 21 reduces to the previous result found for a Tee-section when k_1 is specified as equal to one and k_2 is set equal to zero. Additionally, constraining j equal to one obtains the previous solution for rectangular sections.

The relative density of the lattice can be obtained using the same relationship given by Equation 10. The relative density is a function of lattice geometry (initial curvature, rib length, and rib thickness), and is independent cross-section geometry. A relative stiffness versus relative density plot can be generated by specifying the thermal expansion to be zero, varying the rib aspect ratio, and using numeric methods to maximize the stiffness as a function of the dimensionless cross section constants. Using this technique it was found that the larger the value of *j* becomes, the larger the total stiffness becomes. Additionally stiffness is maximized by allowing k_1 to be equal to 1. For each *j* value, an optimal value for k_2 and m exists which minimizes the required angle theta that results in a zero thermal expansion. Results comparing normalized modulus vs. normalized density for optimized zero expansion triangular lattices with other lattices are shown in **Figure 8**. For example, for a *j* value of 20, relative stiffness improves by a factor of 2.4 for an optimized I section in comparion with a zero expansion lattice with rectangular section ribs.

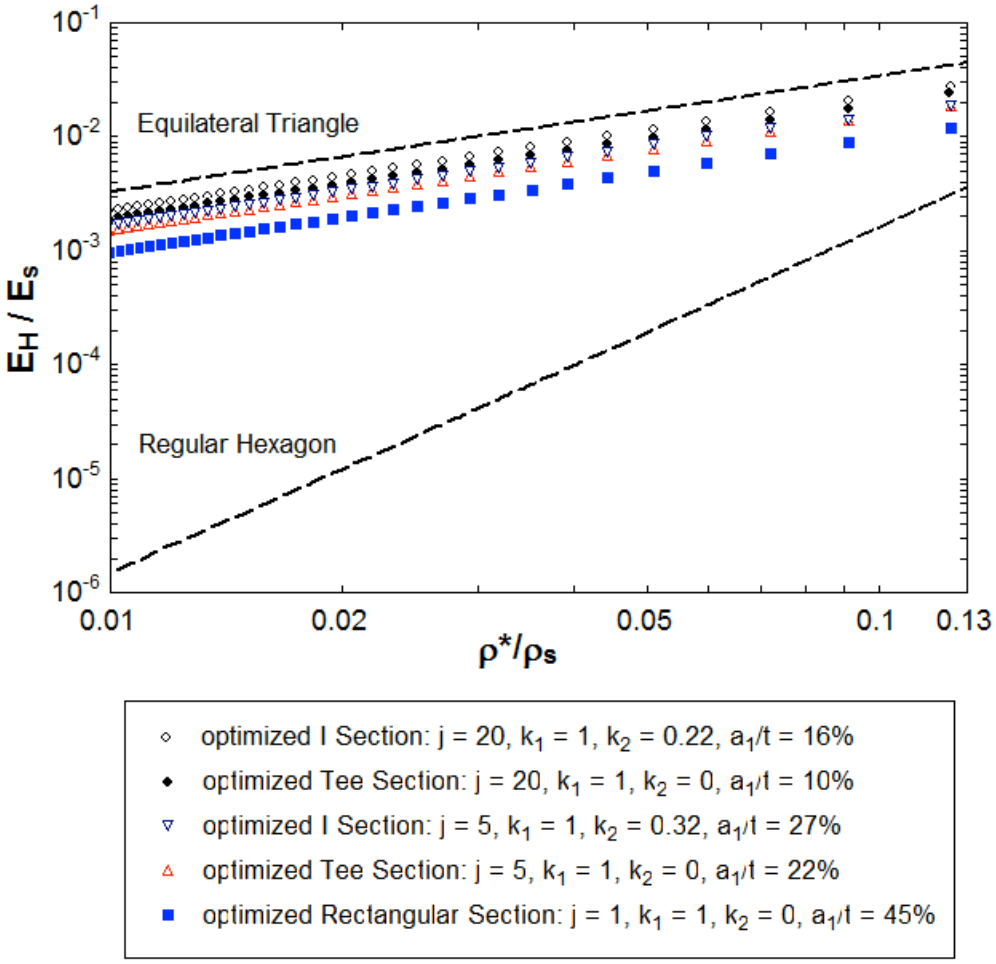

Figure 8 plots relative stiffness versus relative density for zero expansion lattices with several cross sectional shapes. Shapes are optimized for stiffness, for a given value of j and k_1. The dashed lines represent equilateral triangle and regular hexagon lattices, with straight ribs and non-zero thermal expansions.

Thermal Shear Stress γ_T at the Material Interface

A possible limiting factor in the design of curved rib zero expansion bi-material lattices is the shear stress at the material interface. Shear stress develops as a result of the difference in material CTE's. This stress causes bending, which allows for zero thermal expansion. It is desirable to quantify the shear stress and ensure it is not large enough to de-bond materials.

The shear stress is calculated by dividing the shear force, P, by the material interface area A_i. The shear force P is given by Timoshenko (1925), and is shown below in Equation 22. The force P is assumed to be uniformly distributed at the interface. This equation differs from Timoshenko in that it allows for I shaped cross sections having differing distances to the neutral axis (Y_{c1} and Y_{c2}) from the interface, for materials one and two.

$$P = \frac{E_1 I_1 + E_2 I_2}{\rho(Y_{c1} + Y_1)} \qquad \textbf{(22)}$$

ρ represents the change in curvature as a result of the differing CTE's of materials one and two. The interface area (A_i) is dependent upon the dimension less parameters j, k_1, and k_2. It is simplest to restrict the solution to a subset of these dimensionless values. The interface area is given by equation 23, and is valid for *j* values greater than or equal to one, excluding the case of $k_1 = k_2 = 1$. For this subset of sections, which includes rectangular, Tee shaped, and I shaped sections in addition to the sections plotted in **Figure 8**, the interface area is simply L_{arc} times b_2. A new dimensionless parameter X_{10} is defined by equation 24.

$$X_{10} = \frac{t}{L_{arc}} \frac{m\left[(j-1)k_1+1\right]}{(m+1)} \tag{24}$$

Interface shear stress is determined by dividing the shear force by the interface area. The results are given by equation 25.

$$\gamma_T = E_1(\alpha_1 - \alpha_2)\,\Delta T \frac{X_3\, X_{10}}{X_2^2+X_1} \tag{25}$$

Equation 25 was normalized with respect to temperature and solved numerically and plotted to illustrate the effect of *j* and material one thickness percent (a_1/t), as well as to quantify the relative magnitude of the interface shear stress. **Figure 9** plots the interface shear stress versus material one thickness percent, for several *j* values with k_1 equal to 1 and k_2 equal to 0. These curves represent Tee shaped cross sections, where j equals 1 is a rectangular section. Points where stiffness is optimal for the specified j value are shown. **Figure 10** similarly plots interface stresses for various j values, with k_1 equal to 1 and k_2 equal to 0.2 representing I shaped cross sections, where j equals 1 is a rectangular section.

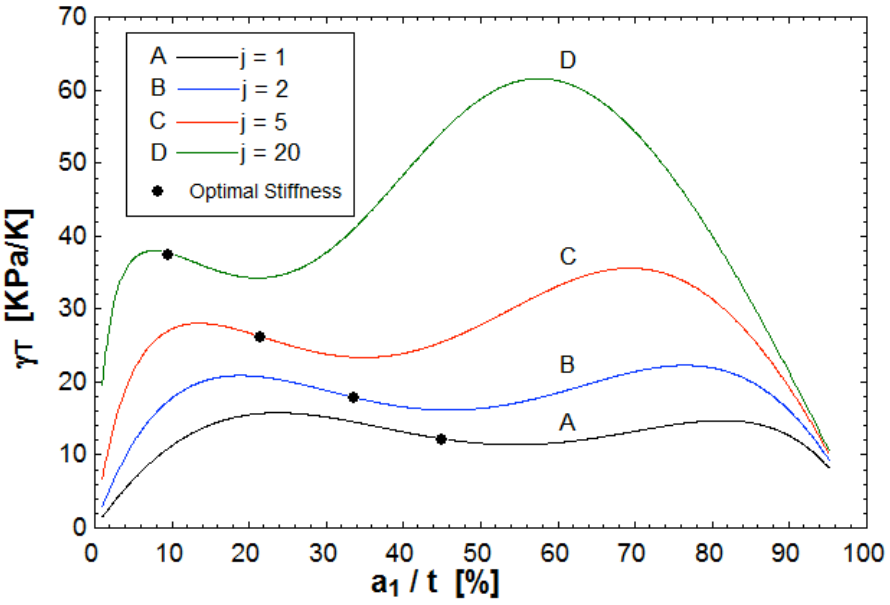

Figure 9 plots temperature normalized interface shear stresses for Tee shaped cross sections. Curve A represents a rectangular section. Markers indicate optimal stiffness configurations.

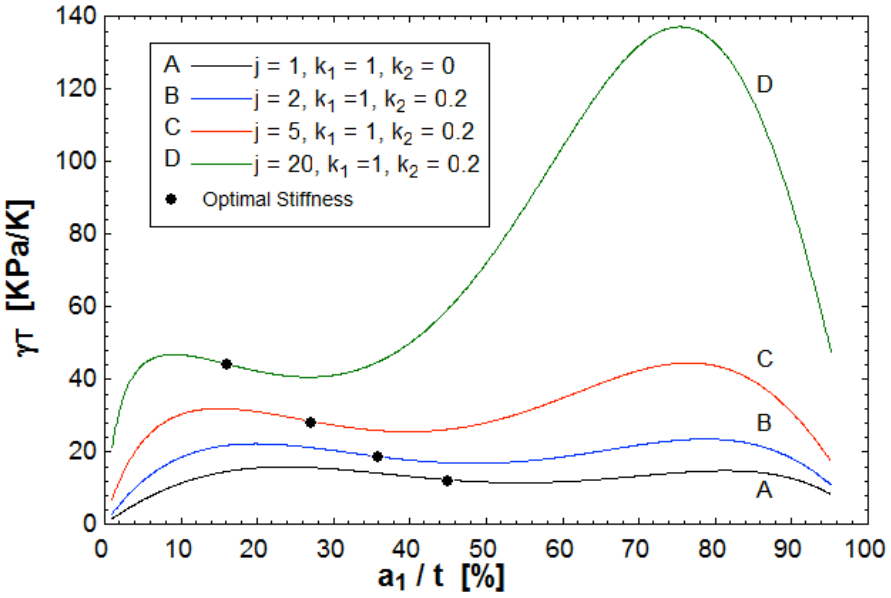

Figure 10 plots temperature normalized interface shear stresses for I shaped cross sections. Curve A represents a rectangular section. Markers indicate optimal stiffness configurations.

The above figures indicate that as the *j* value increases so too does the interface shear stress. This matches what is expected as a result of the material interface area decreasing with increasing *j*. Shear stress is generally larger for I shaped sections of equal *j* values. For a large temperature excursion of 100 K the shear stress for optimized sections is less than 5 MPa, too small to be a problem for bonded metals.

DISCUSSION

Lattices with zero thermal expansion and composed of bi-material ribs are presented. Design of rib cross section shape results in relative stiffness enhancement by a factor of 1.7 for optimized I sections with values of rib section dimension ratio *j* of 5 and a factor of 2.4 for I sections with *j* values of 20 for a given density, compared with ribs of rectangular section. Tee-shaped cross section relative stiffness values increased by a factor of 1.6 for *j* equal to 5 and a factor of 2.1 for *j* equal to 20. These significant increases in relative stiffness are due in large part to increasing the dimensionless parameter *j* from the rectangular section value of 1. A smaller improvement in stiffness is made by specifying an I-section, and choosing an optimum value of parameter k_2. Cross section optimization allows for both stiffer rib elements in bending, as well as decreasing the required curvature needed to achieve zero thermal expansion. This effect is achieved by increasing the geometric stiffness of the Invar relative to that of the steel. With a rib aspect ratio (length/ total thickness) of 10 it is possible to achieve overall stiffness coefficients as high as 14.3 GPa for an optimized I-section with a *j* value of 20, or 10.2 GPa for an I-section with a *j* value of 5. An aspect ratio of 10 for a rectangular section results in a theoretical stiffness value of 6.0 GPa.

The added stiffness is accompanied with an increase in manufacturing complexity, and is further limited by the slenderness and no slip assumptions at the material interface. Shear stresses calculated for Tee shaped and I shaped sections are on the order of 10-40 KPa/K for optimal stiffness configurations. These results are within the realm of practicality, even for a wide range

of temperature values. Cross section optimization results in substantial stiffness improvement at a slight cost of increased interface shear stress.

ACKNOWLEDGEMENT

Support from DARPA-LLNL is gratefully acknowledged.

REFERENCES

Cribb JL (1968) Shrinkage and thermal expansion of a two-phase material. *Nature* 220: 576–577.

L. J. Gibson and M.F. Ashby, (1997), *Cellular Solids*, 2nd edition, Cambridge University Press, Cambridge, UK.

Hashin Z (1983) Analysis of composite materials-a survey. Journal of Applied Mechanics 50: 481–505.

H. E. M. Hunt, (1993), "The mechanical strength of ceramic honeycomb monoliths as determined by simple experiments", *Transactions of the Institution of Chemical Engineers* 71A 257-266.

R. S. Lakes, "Cellular solid structures with unbounded thermal expansion", Journal of Materials Science Letters, **15**, 475-477 (1996).

R. S. Lakes, "Solids with tunable positive or negative thermal expansion of unbounded magnitude", Applied Phys. Lett. 90, 221905 (2007).

J.L. Lehman and R.S. Lakes, (2012), "Stiff Lattices with Zero Thermal Expansion", (accepted for publication in the *Journal of Intelligent Material Systems and Structures*).

Milton G (2002) *The Theory of Composites*. Cambridge University Press, Cambridge, UK.

Paul B (1960) Prediction of elastic constants of multiphase materials. *Transactions of the Metallurgical Society of AIME* 218: 36–41.

Sokolnikoff IS (1983) Mathematical Theory of Elasticity. 2nd ed. Malabar, FL: Krieger.

S. P. Timoshenko, (1925), "Analysis of bi-metal thermostats", *J. Optical Soc. America*, **11,** 233-35.

W. C. Young, (1989). *Roark's Formula's for Stress and Strain* (6th ed.). New York: McGraw-Hill Book company.